International Symposium
On Turbulence and Shear Flow
Phenomena (TSFP-9)
June 30 - July 3, 2015 *Melbourne, Australia*

Spatio-temporal structure of organized motion in turbulence logarithmic layer which mimics the neutral atmospheric surface layer

Yasuo Hattori
Civil engineering research laboratory
Central Research Institute of Electric Power Industry
1646 Abiko, Abiko-shi, Chiba-ken, 270-1194, Japan
yhattori@criepi.denken.or.jp

Hitoshi Suto
Civil enginnering research laboratory
Central Research Institute of Electric Power Industry
1646 Abiko, Abiko-shi, Chiba-ken, 270-1194, Japan
suto@criepi.denken.or.jp

Hiromaru Hirakuchi
Civil engineering research laboratory
Central Research Institute of Electric Power Industry
1646 Abiko, Abiko-shi, Chiba-ken, 270-1194, Japan
hiromaru@criepi.denken.or.jp

ABSTRACT

The temporal- and spatial-structures of the very large-scale coherent structures with organized motions in the logarithmic layer under influences of overlying detached eddies, which mimics the near-neutral atmospheric surface layer, were investigated by using a dynamic PIV measurement. Special attention was paid the dynamic processes of organized motions. The spatial structures of organized motions roughly agree with those conjectured by using time-series of snapshots and Taylor's hypothesis with convective velocity, the value of which was set to time average velocity. The characteristics length of streak structures with low-momentum regions elongated in the streamwise direction exceeded $10h_s$ (h_s: logarithmic layer height). Such characteristics scales of coherence structures normalized with h_s, which corresponds to the atmospheric surface layer height, is consistent with those observed at real sites. This supports the analogy of wind tunnel experiments to the real atmospheric surface layer. The time-series of snapshots clearly shows the coexistence of conflicting two mechanism for turbulence generation due to top-down and bottom up processes (streak structures) reported in previous studies, and the effects of the top-down process on the life-time (characteristics length in streamwise direction) of streak structures.

INTRODUCTION

Comprehension of structural characteristics of organized motions with wind fields in the atmospheric surface layer (ASL), which is a lower part of the atmospheric boundary layer, under near neutral conditions provides a deep insight into coherence structures of high Reynolds number wall turbulences. The ASL easily yields turbulence flows, the Reynolds number of which is much larger than those with wind tunnels. In fact, a renowned observation campaign at the Surface Layer Turbulence and Environmental Science Test (SLTEST) facility (Kunkel and Marusic 2006) used to examine the turbulence structures under very high Reynolds number conditions and have revealed the existence of inherent structures, such as very large-scale organized motions in the logarithmic layer (Hutchins and Marusic 2007, Marusic et al. 2010).

Also, accurate descriptions for turbulence statistics of wind fields in the near-neutral ASL is critically required in view of the increasing and broadening use of numerical weather prediction models. The models need to estimate turbulence fluxes of momentum, heat and moisture in the ASL as boundary conditions. On the other hand, recent observations (Högström 1990, Högström et al. 2002, Drobinski et al. 2004, Drobinski et al. 2007) have indicated that the fluxes under near-neutral conditions are often inconsistent with Monin-Obukhof theory, which has been widely used in the models; the observations were conducted over flat surfaces with homogeneous roughness, and thus the violation from the theory might not be due to the underlying surface conditions.

Possible mechanisms for such deviations from Monin-Obukhof theory have been investigated with the help of rapid distortion theory and large eddy simulations (Högström et al. 2002; Carlotti and Drobinski 2004; Foster et al. 2006; Drobinski et al. 2007). These studies suggest that effects of detached eddies, the characteristics length of which is much larger than those generated by the

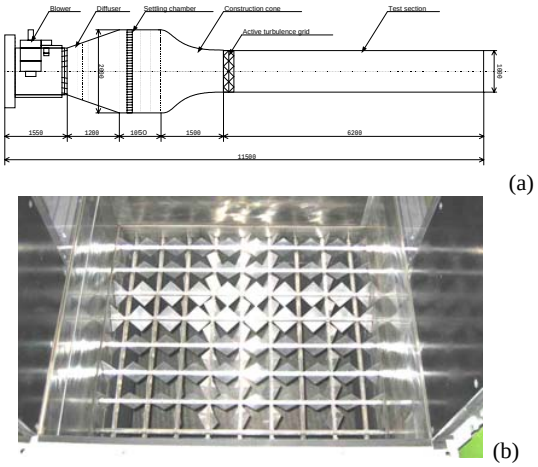

(a)

(b)

Figure 1. Schematics of wind tunnel (a), and picture of active turbulence grid (b).

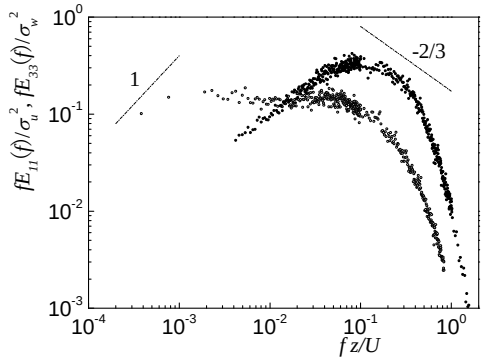

Figure 2. Power spectra of streamwise- and vertical-velocities fluctuation near the surface (at $z/h_s = 0.1$). Open and closed are for streamwise and vertical-velocities.

wind shear in the ASL, on the ASL are essential to the peculiar turbulence characteristics; detached eddies might produce eddy impingements onto the ASL; as they descend into the ASL, they are strongly distorted by the local shear and impinge onto the ASL and change the vertical turbulence transport non-locally.

However, how detached eddies interact with turbulence structures in the ASL is not fully understood; indeed, there has been no clear evidence to show impinging eddy motions that might be key in the ASL and more work is eagerly awaited (Drobinski et al. 2007). In particular, the details of dynamic process, such as generation and disappearance of organized motions with the effects or detached eddies, has not been fully understood yet. This must be due to the lack of the information on spatial- and temporal-structures in the ASL with the observations, which is caused by the difficulty in measuring or including detached eddies in observations or in large-eddy simulations.

Thus, aiming to accumulate a better understanding on interaction between detached eddies and coherence structures with organized motions, we carry out a wind tunnel experiment on the logarithmic layer along a smooth flat plate with detached eddies, which mimics the near-neutral atmospheric surface layer (Hattori et al. 2010). We examine time-series of velocity fields in a horizontal plane by using a dynamic PIV technique, and discuss the dynamic process, such as generation and disappearance of organized motions with time-series of snapshots. Also, we apply a LES filtering procedure (Sullivan et al. 2003, Inagaki and Kanda 2010) for snapshots to discuss the vortex behaviour in the subfilter-scale, which must be helps to improve SGS models used in LES's for atmospheric boundary layer.

EXPERIMENTAL SETUP

We used the same experimental technique of our previous study (Hattori et al. 2010), except velocity measurements. The experiment was conducted in an open-circuit wind tunnel at the Central Research Institute of Electric Power Industry (CRIEPI), as shown in Fig. 1. The test section is 1000 × 1000 mm^2 in area and 6200 mm long, and the walls of the test section are made of smooth flat wood plates. An active turbulence grid, installed at the front of the test section, was used to control the turbulence characteristics in the logarithmic layer; the active turbulence grid composed of rotating grid bars with attached triangular agitator wings, stepping motors located at the end of each grid bards outside the wind tunnel and a controller.

The velocity at the centerline of the test section, U_e, was set to 5 m s^{-1} to obtain the fully-developed turbulence boundary layer at the measuring location, which was fixed at the downstream distance from the active turbulence grid, x, of 4180 mm. The parameters of the active turbulence grid were set such that the normalized profiles of turbulence statistics, including higher-order moments, in the logarithmic layer that have similar to that typically observed in the near-neutral surface layer turbulence. The detailed discussion of comparison of statistics between the experiment and observations, have been reported in our previous paper (Hattori et al. 2010). The logarithmic layer height, h_s, and the friction velocity, u_τ, which are characteristic length and velocity for the logarithmic layer flow, were 70 mm and 0.2 m s^{-1}, respectively. Notice that, the disturbances by the active turbulence grids mainly effects the logarithmic layer height with the reduction in wake region, i.e., the values of h_s and u_τ are 20 mm and 0.17 m s^{-1}, respectively. Also, the values of boundary layer thickness δ defined at the height where the mean velocity is $0.99U_e$, and the momentum thickness θ estimated from momentum loss due to the surface drag are 170 mm and 9 mm, respectively. This boundary layer yields the Reynolds number based on θ ($=U_e\theta/\nu$) exceeding 2.3×10^3, which is in the Reynolds number independent regime. Figure 2 depicts the power spectra of streamwise- and vertical-velocity fluctuations $fE_{11}(f)$ and $fE_{33}(f)$ near the surface ($z/h_s = 0.1$, where z is the vertical distance from the surface), normalized by σ_u, σ_w, z, and mean velocity U at z. The velocity fluctuations were

Figure 3. Example of snapshot of visualized image of horizontal plane in the logarithmic layer; flow direction is upward.

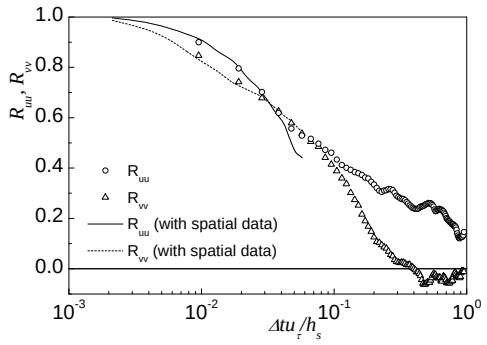

Figure 4. Auto correlations of streamwise and spanwise velocity fluctuation; the curves estimated by two-point correlations with Taylor's hypothesis and convective velocity are also shown.

measured by an x-type hot wire anemometer (Hattori et al. 2010). At the intermediate frequencies, $10^{-3} < fz/U < 10^{-1}$, the spectrum of u shows a plateau while that of w continues to increase with frequency. In the high frequency region $fz/U > 10^{-1}$, $fE_{11}(f)$ and $fE_{33}(f)$ show an inertial sub-range with a constant slope. These profiles agree well with those of observations by Högström et al. (2002), Drobinski et al. (2004), and Kunkel and Marusic (2006). Here I must stress that the power spectra even near the surface ($z/h_s = 0.1$) give inertial sub-range, but also rapidly decay due to viscous effects in the very high frequency region. This implies the the Reynolds number dependency on the footprints of organized motions near the surface. The discussion of the near-surface footprints must be important issue and should be discussed in the future works.

The velocity vectors were measured with a dynamic PIV technique. Figure 3 shows an example of visualized flow fields. Olive-oil mists added to the boundary layer flow were illuminated by light sheet discharged from an YLF laser system, the output of which is 40 W, and the two-dimensional velocity fields in the streamwise-horizontal (x-y) plane at z = 30 mm (= $0.43h_s$) were visualized. Particle-containing flow images with a physical size of 150 × 150 mm^2 ($\cong 2h_s \times 2h_s$) were captured by a high-speed camera (1028 × 1028 pixel^2) with the sampling frequency of 300 Hz. Then, the velocity vectors were calculated using a cross-correlation method with interrogation windows of a size of 32 × 32 pixel^2. The overlap ratio was 50%, and the 4096 velocity vectors were obtained in each pair of images, providing the spatial resolution of $0.03h_s \times 0.03h_s$. A sub-pixel algorithm assuming a Gaussian profile for the spatial correlation was also applied to improve the dynamic spatial range of velocity vectors. After calculating velocity vectors, incorrect velocity vectors were removed with a medial filter, and empty data grids were filled with interpolated velocity vectors. Statistics were calculated from velocity vectors obtained with about 18000 image pairs. The accuracy of the PIV measurement was verified as follows. Turbulence measurement was also carried out with the x-type hot wire anemometer (Hattori et al. 2010); we confirmed that the turbulence statistics measured from PIV agreed well with those from the hot wire: the estimated uncertainties (95% coverage) were 3.7% for the time averaged value, and 6.8% for the r.m.s. value of streamwise velocity respectively. Also notice that, the logarithmic layer height h_s, is used here as the characteristics length scale on normalizing measurements, because (1) this study focuses on just the ASL, and (2) experiment does not simulate the outer layer well and cannot be used to estimate the whole boundary layer thickness, which is often used scale atmospheric data. Also, I must stress that the length with fluid viscosity, which is usually used for wall turbulences, is not suitable for the ASL; the atmospheric data have been handled with the turbulence fluxes conditions at the surface (no-slip conditions are not generally used).

RESULTS

Figure 4 presents the auto-correlations of streamwise and spanwise velocity fluctuations, R_{uu} and R_{vv}. The time difference Δt is normalized with h_s and u_τ. The values calculated by using the spatial data (in the visualized plane, the size of which is $2h_s \times 2h_s$) with the Taylor's hypothesis are also shown; here, the convective velocity, U_c, was set to time-averaged streamwise velocity ($U_c/u_\tau = 15.7$). The auto-correlations with temporal data agree well with those with spatial data, while R_{uu} for $\Delta t u_\tau/h_s > 5 \times 10^{-2}$ shows some differences. This implies the validity of Taylor's hypothesis in constructing spatial structures of organized motions, which corresponds to the previous study by Dennis and Nickels (2008). The decay of R_{uu} against Δt is very slow: R_{uu} preserves significant values at $\Delta t u_\tau/h_s = 6 \times 10^{-1}$. This indicates the existence of streaky structures with highly elongated region of uniform streamwise momentum that yields the characteristics length of $10h_s$.

Figure 5 depicts a typical example of time-series of contour of instantaneous streamwise velocity. The flow direction is upward in the figure; the warm- and cold-colours (the ranges of colour bar are fixed), refer to high- and low-speed regions. Note that, these contours present the spatial structures in organized motions: sequence is from top to bottom; the normalized time step $\Delta t u_\tau/h_s$ is set

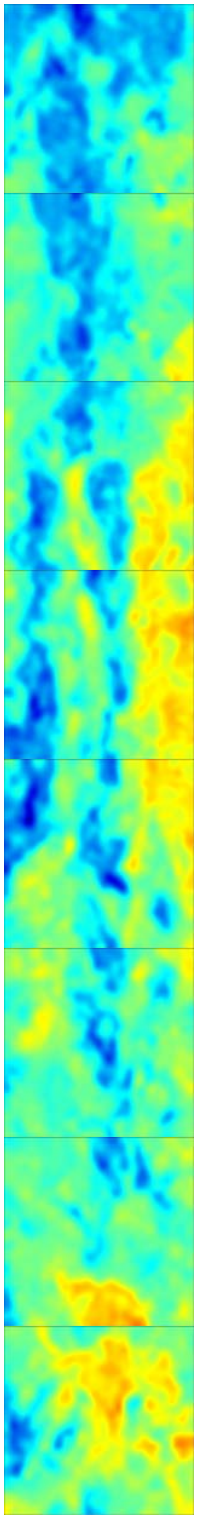

Figure 5. Time-series of contour of instantaneous streamwise velocity; flow direction is upward; normalized time step is set to 9.6×10^{-2} (=1/30 s); sequence is from top to bottom; warm and cold colours refer to large and small value region

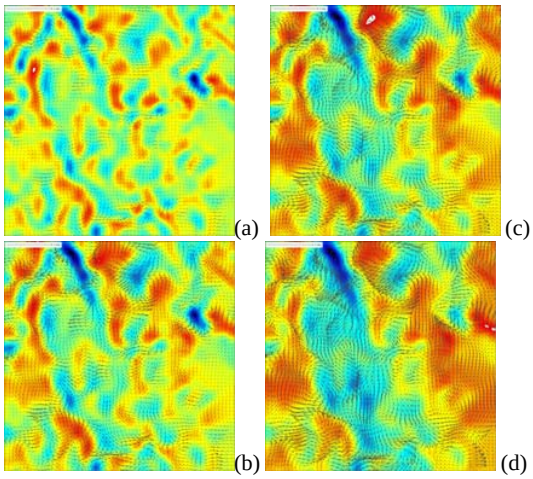

Figure 6. Vectors and contours of instantaneous velocities with streaky structures filtered with filter width of Δ_f = $h_s/16$, (a) , $h_s/8$, (b), $h_s/4$, (c), and $h_s/2$, (d).

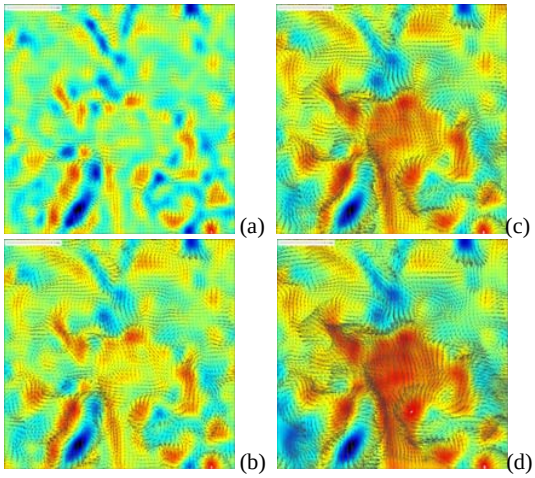

Figure 7. Vectors and contours of instantaneous velocities with cat paw's interact filtered with filer width of Δ_f = $h_s/16$, (a) , $h_s/8$, (b), $h_s/4$, (c), and $h_s/2$, (d).

to 9.1×10^{-2} (= 1/30 s) which gives the convection distance that corresponds to the physical size of visualized image by using Taylor hypothesis with convective velocity (U_c/u_τ = 15.7). The low-speed regions elongated in the streamwise direction are observed. These regions are also accompanied by high-speed regions, which are developed with convection of low-speed regions downstream. These processes yield the streaky structures; the spanwise spacing between low- and high-speed regions is about $0.5h_s$. The length of streaky structures in streamwise direction is roughly estimated to $10h_s$. These characteristics lengths are consistent with the observation in the near-neutral ASL (Drobinski et al. 2007; Hutchins and Marusic 2007; Hutchins et al. 2012). The high-speed area appears after passing the streak structures. The area

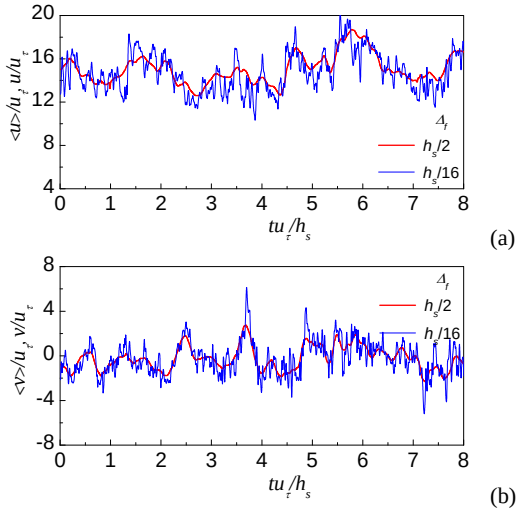

Figure 8. Waveform of velocity of streamwise (a) and spanwise (b) components with filterd width of $\Delta_f = h_s/16$, and $h_s/2$; the velocities include time-averaged values.

has the size of h_s in stream- and spanwise-directions, which might be related to the cat's paw interact due to the impingements of detached eddies onto the logarithmic layer (Hunt and Morrison 2000).

Here, we have utilized a LES filtering procedure to discuss the vortex behaviour in the subfilter-scale, which must be helps to improve SGS models used in LESs for atmospheric boundary layer. We decomposed the instantaneous velocity fields into two, resolved- and sublifter-scales by the application of a top-hat spatial filter (Sullivan et al. 2003, Inagaki and Kanda 2010) with the filter width Δ_f, i.e., the filtered field was calculated by exponentially weighted moving average with the filter widths of Δ_f.

Figures 6 and 7 show the snapshots of vectors and contour of instantaneous velocity of subfilter-scale motions for the time-slices, which give two kinds of coherence structures, streaky structures and cat's paw interact. The filter width Δ_f was varied from $h_s/16$ to $h_s/2$. The range of colour bar of contour changes with filter size changes with Δ_f, while the vector length is fixed. The intensities of velocity fluctuations increase with the filter width Δ_f, as shown in velocity vectors. The contours for $\Delta_f > h_s/4$ exhibit the coherence structures, which generate heterogeneous vortex behaviour: the strong vortex motions appears along the organized motions. Contrary to this, the contours for $\Delta_f < h_s/4$ present homogeneous flow fields with vortex motions.

Figure 8 shows the waveform of streamwise- and spanwise-velocities for $\Delta_f = h_s/16$ and $\Delta_f = h_s/2$. The time-series of contour in Fig. 4 was observed for $tu_\tau/h_s = 2.7 - 3.7$. The high-speed area observed at $tu_\tau/h_s \cong 3.5$, which gives cat' paw interact, yields the increase in ensemble value of streamwise velocity, $\langle u \rangle$, which means the acceleration of flow fields in the whole of logarithmic layer. Thus, such high-speed area might be due to the sweep-like events with detached eddies generated above the ASL (Högström et al. 2002; Hattori et al. 2010). This also supports the coexistence of organized motions with top down process with detached eddies suggested by Hutchins et al (2012).

DISCUSSION AND CONCLUSIONS

The study here examined coherence structures with organized motions in the logarithmic layer with the effects of detached eddies, which mimics the near-neutral atmospheric surface layer (ASL). We carried out a wind tunnel experiment to discuss dynamic processes, such as generation and disappearance of organized motions; the detached eddies were generated by the active turbulence grid (Hattori et al. 2010) and time-series of velocity fields in a horizontal plane in the logarithmic layer were measured by using a dynamic PIV technique. Also, a LES filtering procedure (Sullivan et al. 2003, Inagaki and Kanda 2010) for snapshots were used to grasp the vortex behaviour in the subfilter-scale, which must be helps to improve SGS models used in LES's for atmospheric boundary layer.

The decay of auto-correlations of streamwise velocity fluctuations against time lags agreed well with that of cross-correlations calculated by the spatial data with the Taylor's hypothesis and the convective velocity, which was set to time-averaged velocity. This agreement supports the validity of Taylor's hypothesis in constructing spatial structures of organized motions, corresponding to the previous study by Dennis and Nickels (2008). The decay of the auto-correlations, which was very slow, and also the spatial distributions of instantaneous velocity showed streaky structures with the low-speed regions elongated in the streamwise direction. The characteristics length of such structures exceeded $10h_s$ (h_s: logarithmic layer height). This length normalized with h_s, which corresponds to the ASL height, was consistent with the observations for near-neutral ASL (Drobinski et al. 2007; Hutchins and Marusic 2007; Hutchins et al. 2012). This consistent also supports the analogy of wind tunnel experiments to the real ASL.

The time-series of snapshots and waveforms of streamwise velocity revealed cat's paw interact (Hunt and Morrison 2000) due to impingements of detached eddies with the characteristics length of h_s in streamwise- and spanwise-directions. They indicated the coexistence of conflicting two mechanism for turbulence generation due to top-down and bottom up processes (streak structures) reported in previous studies (Hutchins et al. 2012), and the effects of the top-down process on the life-time (characteristics length in streamwise direction) of streak structures: the characteristics length of streak structure, $10h_s$, is closely related to the profile of power spectrum of streamwise velocity fluctuation, which shows a plateau at intermediate frequencies with effects of detached eddies (Högström et al. 2002).

The vectors and contour of instantaneous velocities of subfilter-scale motions for the filter width $\Delta f < h_s/4$ exhibited homogeneous flow fields where vortex motions become dominant, whereas the filter width $\Delta f > h_s/4$ provided the coherence structures with organized motions, which mainly contributes to turbulence generations in the logarithmic layer. On the other hand, such filter width is

often used in the LES's with numerical weather prediction models as suggested by Sullivan et al. (2003). The correlation between gridscale and subgridscale must be apparently quite weak with such filtering, suggesting that conventional Smagorinsky models, which is widely used in the numerical weather pre-diction models (Moeng et al., 2007), might have some problems for estimating instantaneous subfilter-scale fluxes in the ASL. The existing simulations (e.g. Anderson et al., 2007) have also suggested that the Smagorinsky type models have weakness for representing turbulence statistics in the vicinity of the surface, and developing models, such as dynamic models have been proposed (e.g. Sullivan et al., 2003; Chen et al., 2009). The check for the performance of such newly models must be important issue and should be discussed in the future works.

The authors are deeply indebted to the anonymous reviews for useful comments on the extended abstract. The authors also thank Mr. Takayoshi Mizuno of CERES for his careful assistance in wind tunnel experiments. This work was performed under the support of collaboration between NCAR and CRIEPI; the authors acknowledge Dr. Chin-Hoh Moeng of NCAR and Dr. Keisuke Nakao of CRIEPI for valuable discussion and wish to express our gratitude to Dr. Sun, Juan Zhen and Dr. Soichiro Sugimoto for helps of the collaboration between NCAR.

REFERENCES

Anderson, W. C., Basu, S., Letchford, C. W. (2007) Comparison of dynamic subgrid-scale models for simulations of neutrally buoyant shear-driven atmospheric boundary layer flows. Environmental Fluid Mech, 7, p195-215.

Carlotti, P., Drobinski, P. (2004) Length scales in wall- bounded high-Reynolds-number turbulence. J Fluid Mech 516: 239-264.

Chen, Q., Otte, M. J., Sullivan, P. P., Tong, C. (2009) A posteriori subgrid-scale model tests based on the conditional means of subgrid-scale stress and its production rate. J of Fluid Mech, 626, p149-181.

Dennis, D.J.C., Nickels, T.B. (2008) On the limitations of Taylor's hypothesis in constructing long structures in a turbulent boundary layer. J Fluid Mech, 614, p197-206.

Drobinski, P., Carlotti, P. Newsom, R.K., Banta, R.M., Foster, R.C., Redelsperger, J-L. (2004) The structure of the near-neutral atmospheric surface layer. J Atmos Sci, 61, p699-714.

Drobinski, P., Carlotti, P., Redelsperger, J-L., Banta, R.M., Masson, V., Newsom, R. (2007) Numerical and experimental investigation of the neutral atmospheric surface layer. J Atmos Sci, 64, p137-156.

Foster RC, Vianey F, Drbinski P, Carlotti P (2006) Near-surface coherent structures and the vertical momentum flux in a large-eddy simulation of the neutrally-stratified boundary layer. Boundary-Layer Meteorol 120: 229-255.

Hattori, Y., Moeng, C-H. Suto, H., Tanaka, N., Hirakuchi, H. (2010) Wind-tunnel experiment on logarithmic-layer turbulence under the influence of overlying detached eddies. Boundary-Layer Meteorol, 134, p269-283.

Högström, U. (1990) Analysis of turbulence structure in the surface layer with a modified similarity formulation for near neutral conditions. J Atmos Sci, 47, p1949-1972.

Högström, U., Hunt. J.C.R., Smedman, A-S. (2002) Theory and measurements for turbulence spectra and variances in the atmospheric neutral surface layer. Boundary-Layer Meteorol, 103, p101-124.

Hunt, J.C.R., Morrison, J. F. (2000) Eddy structure in turbulent boundary layers. Eur J Mech B-Fluids, 19, p673-694.

Hutchins, N., Marusic, I. (2007) Evidence of very long meandering features in the logarithmic region of turbulent boundary layers. J Fluid Mech, 579, p1-28.

Hutchins, N., Chauhan, K., Marusic, I., Monty, J., Klewicki, J. (2012) Towards reconciling the large-scale structure of turbulent boundary layers in the atmosphere and laboratory. Boundary-Layer Meteorol, 145, p273 - 306.

Inagaki, A., Kanda, M. (2010) Organized structure of active turbulence over an array of cubes within the logarithmic layer of atmospheric flow. Boundary-Layer Meteorol,135, p209-228.

Kunkel, G.J., Marusic, I. (2006) Study of the near-wall-turbulent region of the high- Reynolds-number boundary layer using an atmospheric flow. J Fluid Mech, 548, p375-402.

Marusic, I., Mathis, R., Hutchins, N. (2010) Predictive model for wall-bounded turbulent flow. Science, 329, p193-196.

Moeng, C.-H., Dudhia, J., Klemp, J., Sullivan, P.P (2007) Examining two-way grid nesting for large eddy simu-lation of the PBL using the WRF model. Monthly Weather Rev, 135, pp2295-2311.

Sullivan, P. P., Horest, T. W., Lenschow, D. H., Moeng, C-H., Weil, J .C. (2003) Structure of subfilter-scale fluxes in the atmospheric surface layer with application to large-eddy simulation modeling. J Fluid Mech, 482, p101-139.